Materials Advances

ROYAL SOCIETY
OF CHEMISTRY

PAPER
Yousuke Ooyama *et al.*
Organohalogenochromism (OHC) of D–π–A pyridinium
dye polymer films and the colorimetric detection of volatile
organic halogen compounds

PAPER

Check for updates

Organohalogenochromism (OHC) of D−π−A pyridinium dye polymer films and the colorimetric detection of volatile organic halogen compounds†

Kumpei Kozuka, Keiichi Imato [ID] and Yousuke Ooyama [ID] *

Volatile organohalogen compounds (VOHCs) are commonly used in manufacturing; however, most of them are extremely toxic to human health, biological systems and the environment even when exposed to small quantities. Meanwhile, organohalogenochromism (OHC) is a photophysical phenomenon that induces a significant hypsochromic or bathochromic shift of photoabsorption bands of organic dyes in halogenated solvents compared with those in non-halogenated solvents. Thus, in this study, to ensure the expression of OHC and to develop optical polymeric materials based on OHC for the visualization and detection of VOHCs, we designed and synthesized a D−π−A type pyridinium dye monomer **OD2-V** possessing intramolecular charge transfer (ICT) characteristics and prepared a copolymer **poly(OD2-*co*-S)** composed of **OD2-V** and styrene. It was found that **poly(OD2-*co*-S)** and **OD2-V** exhibit bathochromic shift-type OHC (b-OHC) in the solution state. However, the D−π−A type pyridine dye **NI2-V** and its copolymer **poly(NI2-*co*-S)** composed of **NI2-V** and styrene did not exhibit such OHC. Furthermore, drop-casted **poly(OD2-*co*-S)** film exhibits the bathochromic shift of the ICT-based photoabsorption band in the halogenated solvent−vapor atmosphere, that is, a visual change in color from yellow to orange upon exposure to VOHCs, including dichloromethane (CH_2Cl_2) and chloroform ($CHCl_3$). Indeed, the **poly(OD2-*co*-S)** film exhibits a good reversible switching of the ICT-based photo-absorption band in the air and VOHC-vapor atmosphere process. The optical sensing properties of **poly(OD2-*co*-S)** film to VOHCs, ^{1}H NMR spectral measurements and semi-empirical molecular calculations for **OD2-V** demonstrate that the enhanced ICT characteristics of **OD2** chromophore induced by the intermolecular interaction between the dye and the organohalogen molecules are responsible for the b-OHC of D−π−A type pyridinium dyes. Consequently, we propose that polymeric organohalogenochromic dyes are one of the most promising and convenient functional materials for the colorimetric detection of VOHCs.

Introduction

Organohalogenochromism (OHC) has recently been recognized as a photophysical phenomenon that induces a significant hypsochromic or bathochromic shift of the photoabsorption bands of organic dyes in halogenated solvents compared with those in non-halogenated solvents.[1–4] Hence, OHC is a specific solvatochromism observed only in halogenated solvents that is different from a common solvatochromism depending on the dielectric constant (ε_r) of solvent and solvent polarity parameter $E_T(30)$; it can be actually classified into two types, positive solvatochromism (p-SC) and negative solvatochromism (n-SC), which correspond to a bathochromic shift and a hypsochromic shift, respectively, with increasing solvent polarity.[5–12] Batho-chromic shift-type OHC (b-OHC) has been occasionally found in donor−π−acceptor (D−π−A) type dyes, which are composed of dialkyl or diaryl amino groups as a strong electron-donating moiety (D) and pyridinium, benzothiazolium, dicyanomethyl-ene, and barbituric moieties as a strong electron-withdrawing moiety (A) connected by a π-conjugated bridge, and it can exhibit a photoabsorption band based on the intramolecular charge transfer (ICT) from the D moiety to the A moiety.[1–4,13–28] However, few studies have been carried out on OHC although the phenomenon is of great scientific interest and practical importance, such as the development of optical sensors for the detection of toxic organohalogen compounds.[29–35] Actually, volatile organohalogen compounds (VOHCs) are commonly used in manufacturing,[36–43] but most of them are extremely

Applied Chemistry Program, Graduate School of Advanced Science and Engineering, Hiroshima University, 1-4-1 Kagamiyama, Higashi-Hiroshima 739-8527, Japan. E-mail: yooyama@hiroshima-u.ac.jp

toxic to human health, biological systems and the environment even when exposed to small quantities. Several detection techniques for VOHCs have been developed, including gas chromatography–mass spectrometry (GC–MS) and gas chromatography-flame ionization detector (GC-FID) methods.[44–47] Although these techniques provide sufficient qualitative and quantitative accuracy, they generally require time-consuming procedures for sample preparation and sophisticated experimental skills for operation and analysis as well as expensive instrumentation. The development of optical detection techniques for VOHCs based on organic dyes, which involve facile operation and simple analysis, allows not only sufficient accuracy, high sensitivity, and fast response but also allows the visualization and real-time monitoring of VOHCs. Thus far, we have focused on the elucidation of OHC and the creation of functional dye materials based on OHC for visualization and detection of organohalogen compounds.[1–4] In our previous work,[2] we developed D–π–A type pyridinium dyes **OD1–3** bearing a halide anion (X⁻ = Cl⁻, Br⁻, or I⁻) as the counter anion and investigated their photophysical properties in various solvents (Fig. 1a). It was found that **OD1–3** showed a b-OHC, that is, the significant bathochromic shift of the ICT-based photoabsorption band in halogenated solvents although the semi-empirical molecular orbital (MO) calculations predicted that **OD1–3** will show n-SC. Based on the ^{1}H NMR spectroscopic studies of **OD1–3** in deuterated non-halogenated solvents and deuterated halogenated solvent, it was suggested that the enhanced ICT characteristics of **OD1–3** in halogenated solvents, which might be induced by the formation of halogen–halide anion interaction[48–50] between the halogen atoms of halogenated solvents and the counter halide anion of the dye, are responsible for the b-OHC of D–π–A type pyridinium dyes bearing a counter anion. Moreover, the b-OHC is observed for non-ionic D–π–A dyes with dicyanomethylene and barbituric moieties as a strong electron-withdrawing group,[18–20] but their OHC remains poorly elucidated. Therefore, to create organohalogenochromic dye materials for the

visualization and detection of VOHCs, it is necessary to further investigate the effects of intermolecular interaction between the dyes and the organohalogen molecules, including halogen–π interaction[51–55] between halogen atoms of halogenated solvents and aromatic π-systems of dye molecules as well as halogen–halide anion interaction.[48–50]

Thus, in this work, to ensure the expression of OHC and to develop optical polymeric materials based on OHC for the colorimetric detection of VOHCs, we designed and synthesized a D–π–A type pyridinium dye monomer **OD2-V** with a vinyl group on the carbazole skeleton as a derivative of **OD2** and prepared a copolymer **poly(OD2-co-S)** composed of **OD2-V** and styrene (Fig. 1b). It was found that **poly(OD2-co-S)** exhibits b-OHC in the solution state, and its drop-casted film shows the bathochromic shift of the ICT-based photoabsorption band in halogenated solvent–vapor atmosphere, that is, a visual change in color when exposed to VOHCs, including dichloromethane (CH_2Cl_2) and chloroform ($CHCl_3$). The **poly(OD2-co-S)** film exhibits good reversible switching of the ICT-based photoabsorption band in the air and VOHC-vapor atmosphere process. Herein, we report the b-OHC of polymeric organohalogenochromic dye based on the intermolecular interaction between the dye and the organohalogen molecules and the optical sensing properties of its film to VOHCs, which were revealed by comparison with the D–π–A type pyridine dye monomer **NI2-V** and its copolymer **poly(NI2-co-S)** composed of **NI2-V** and styrene.

Results and discussion

Synthesis

D–π–A type pyridinium dye **OD2-V** and a copolymer **poly(OD2-co-S)** composed of **OD2-V** and styrene were prepared according to a stepwise synthetic protocol (Scheme 1). First, **NI2-V** was obtained in moderate yield (64%) by the reaction of **NI2**[56] with n-BuLi, followed by treatment with vinyl bromide in the presence of Pd(dba)₂/2P(t-Bu)₃. Next, the reaction of **NI2-V** with n-butyl bromide gave **OD2-V** in a relatively high yield (78%). Then, polymerization was carried out at a ratio of **NI2-V** to styrene of 1 : 99 using 2,2′-azobis(isobutyronitrile) (AIBN) as a free radical initiator to give **poly(NI2-co-S)** as a white solid (M_n = 59 200, M_w/M_n = 1.55, 8% yield). The ^{1}H NMR spectrum indicated that the molar ratio (x/y) of styrene unit (x) and **NI2-V** unit (y) and the weight percentage (wt%) of **NI2-V** in the obtained **poly(NI2-co-S)** were determined to be ca. 667 and ca. 0.62 wt%, respectively. Finally, the reaction of **poly(NI2-co-S)** with n-butyl bromide gave **poly(OD2-co-S)** as a yellow solid in high yield (84%). The preparation of **poly(OD2-co-S)** was demonstrably confirmed by the FT-IR, the ^{1}H NMR (Fig. S3b and S5b, ESI†) and the photoabsorption spectra (Fig. 3c and d).

Photoabsorption properties

The photoabsorption spectra of **NI2-V**, **OD2-V**, **poly(NI2-co-S)**, and **poly(OD2-co-S)** in various solvents are shown in Fig. 2 and 3, and their photophysical data are summarized in Tables 1 and 2.
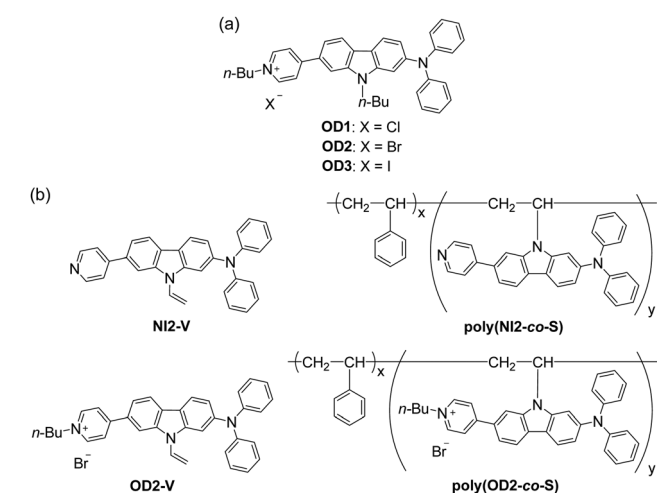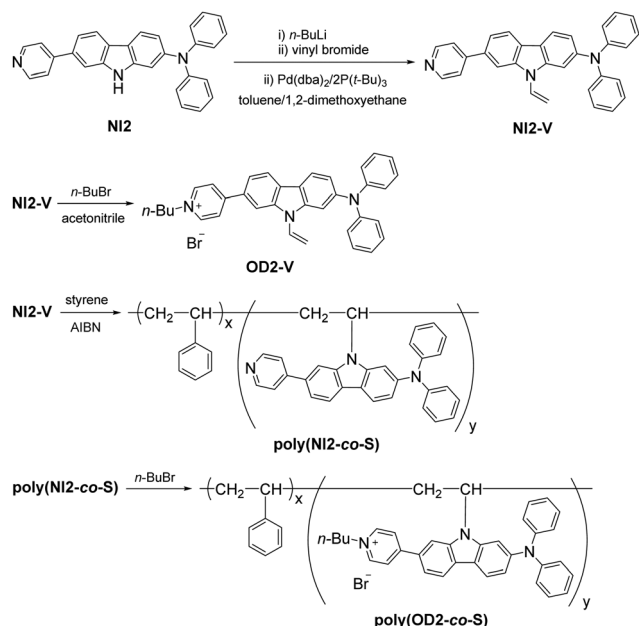

Fig. 1 Chemical structures of (a) D–π–A type pyridinium dyes **OD1–3** possessing organohalogenochromic characteristics (previous work) and (b) D–π–A type pyridine dye monomer **NI2-V**, D–π–A type pyridinium dye monomer **OD2-V**, and their copolymer **poly(NI2-co-S)** and **poly(OD2-co-S)** composed of the dye monomer and styrene (in this work).

Scheme 1 Synthesis of **NI2-V**, **OD2-V**, **poly(NI2-co-S)**, and **poly(OD2-co-S)**.
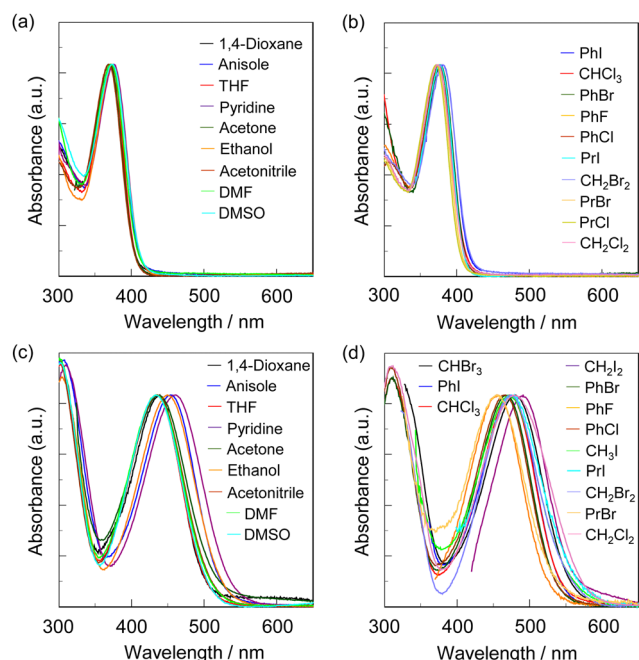

Fig. 2 Photoabsorption spectra of (a) **NI2-V** and (c) **OD2-V** in non-halogenated solvents and (b) **NI2-V** and (d) **OD2-V** in halogenated solvents.

Fig. 3 Photoabsorption spectra of (a) **poly(NI2-co-S)** and (c) **poly(OD2-co-S)** in non-halogenated solvents and (b) **poly(NI2-co-S)** and (d) **poly(OD2-co-S)** in halogenated solvents.

The photoabsorption bands in the visible region appeared at around 350–400 nm for **NI2-V** and **poly(NI2-co-S)** and 400–550 nm for **OD2-V** and **poly(OD2-co-S)**, which are attributed to ICT excitation from the (diphenylamino)carbazole unit as a D–π moiety to a pyridine ring or pyridinium ring as an A moiety, which is supported by the semi-empirical MO calculations, as discussed later. The ICT-based photoabsorption maximum
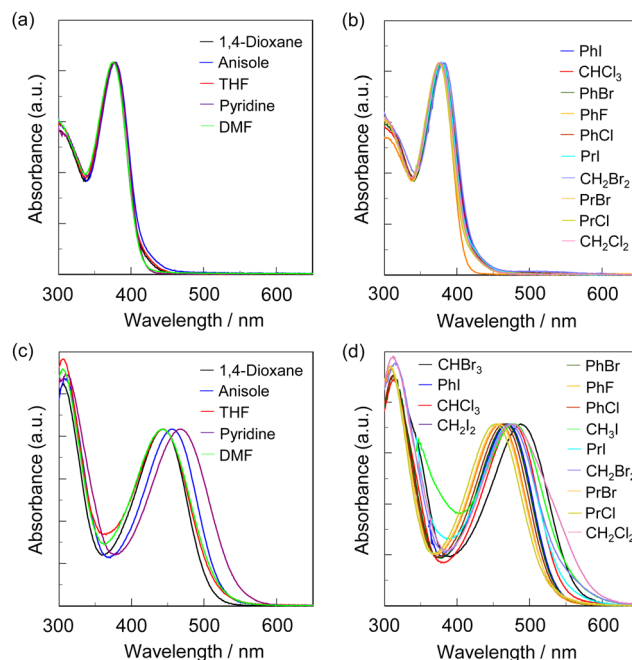
wavelength $\lambda_{\mathrm{max(exp)}}^{\mathrm{abs\text{-}solution}}$ (*ca.* 430–490 nm) of **OD2-V** and **poly(OD2-co-S)** showed a large bathochromic shift owing to the strong electron-withdrawing ability of the pyridinium ring compared with those ($\lambda_{\mathrm{max(exp)}}^{\mathrm{abs\text{-}solution}}$ = 370–380 nm) of **NI2-V** and **poly(NI2-co-S)**, and the ε values (*ca.* 20 000–40 000 M^{-1} cm^{-1}) for **NI2-V** are higher than those (*ca.* 10 000–25 000 M^{-1} cm^{-1}) for **OD2-V**. The photoabsorption spectra of **NI2-V** and **poly(NI2-co-S)** are nearly independent of the kinds of solvents (Fig. 2a, b and 3a, b), but those of **OD2-V** and **poly(OD2-co-S)** depend on the categories of solvents. In particular, it is worth noting that **OD2-V** and **poly(OD2-co-S)** show a significant bathochromic shift of $\lambda_{\mathrm{max(exp)}}^{\mathrm{abs\text{-}solution}}$ in halogenated solvents compared with those in non-halogenated solvents (Fig. 2c, d and 3c, d), that is, a pronounced b-OHC as with the previously reported D–π–A pyridinium dye **OD2**[2] (Fig. 1a). Indeed, for **NI2-V**, the rage of $\lambda_{\mathrm{max(exp)}}^{\mathrm{abs\text{-}solution}}$ is from 369 nm in acetone or acetonitrile to 381 nm in iodobenzene (PhI) for all the solvents and from 369 nm in acetone or acetonitrile to 376 nm in pyridine for non-halogenated solvents, but for **OD2-V**, it is from 433 nm in DMSO to 491 nm in CH$_2$I$_2$ for all the solvents and from 433 nm in DMSO to 461 nm in pyridine for non-halogenated solvents. Therefore, for **NI2-V**, the difference ($\Delta\lambda_{\mathrm{max(exp)}}^{\mathrm{abs\text{-}solution}}$) between the shortest and longest $\lambda_{\mathrm{max(exp)}}^{\mathrm{abs\text{-}solution}}$ values is 12 nm (853 cm^{-1}) for all the solvents and 7 nm (504 cm^{-1}) for non-halogenated solvents, but for **OD2-V**, it is 58 nm (2728 cm^{-1}) for all the solvents and 28 nm (1402 cm^{-1}) for non-halogenated solvents (Table 1). Similarly, the $\Delta\lambda_{\mathrm{max(exp)}}^{\mathrm{abs\text{-}solution}}$ values for all the solvents and non-halogenated solvents are, respectively, 7 nm (488 cm^{-1}) and 4 nm (281 cm^{-1}) for **poly(NI2-co-S)** and 45 nm (2081 cm^{-1}) and 26 nm (1251 cm^{-1}) for **poly(OD2-co-S)** (Table 2).

Table 1 Experimental and calculational photophysical data of **NI2-V** and **OD2-V** in various solvents

No.	Solvents	$\varepsilon_r{}^a$	$E_T(30)^b$/ kcal mol^{-1}	NI2-V $\lambda_{max(exp)}^{abs\text{-}solution}$/nm ($\varepsilon$/M^{-1} cm^{-1})	NI2-V $\lambda_{max(calc)}^{abs\text{-}solution}$/nm ($f^f$)	OD2-V $\lambda_{max(exp)}^{abs\text{-}solution}$/nm ($\varepsilon$/M^{-1} cm^{-1})	OD2-V $\lambda_{max(calc)}^{abs\text{-}solution}$/nm ($f^f$)
1	1,4-Dioxane	2.22	36.0	373 (27 000)	353 (0.88)	439 (—[e])	440 (1.01)
2	Anisole	4.30	37.1	375 (32 000)	356 (0.88)	454 (20 900)	398 (1.14)
3	CHBr$_3$	4.40	37.7	—[d]	356 (0.88)	481 (25 900)	396 (1.14)
4	PhI	4.59	36.2	381 (20 700)	357 (0.88)	473 (23 200)	394 (1.15)
5	CHCl$_3$	4.81	39.1	376 (26 600)	355 (0.89)	472 (26 100)	396 (1.15)
6	CH$_2$I$_2$	5.32	36.5	—[d]	358 (0.88)	491 (10 900)	387 (1.18)
7	PhBr	5.45	36.6	378 (16 000)	357 (0.88)	467 (—[e])	390 (1.18)
8	PhF	5.47	37.0	373 (32 800)	356 (0.89)	455 (—[e])	391 (1.17)
9	PhCl	5.69	36.8	376 (23 800)	356 (0.89)	466 (—[e])	388 (1.18)
10	CH$_3$I	6.97	—[c]	—[d]	357 (0.89)	473 (14 000)	383 (1.21)
11	1-Iodopropane (PrI)	7.07	35.7	377 (26 700)	357 (0.89)	475 (—[e])	383 (1.21)
12	THF	7.52	37.4	372 (20 800)	356 (0.89)	434 (24 000)	382 (1.21)
13	CH$_2$Br$_2$	7.77	39.4	380 (26 600)	357 (0.89)	473 (18 000)	380 (1.22)
14	1-Bromopropane (PrBr)	8.09	36.9	374 (42 000)	356 (0.89)	456 (—[e])	382 (1.21)
15	1-Chloropropane (PrCl)	8.59	37.4	372 (28 300)	356 (0.89)	—[e]	382 (1.22)
16	CH$_2$Cl$_2$	8.93	40.7	373 (18 100)	356 (0.89)	477 (16 400)	383 (1.21)
17	Pyridine	13.3	40.5	376 (25 000)	358 (0.89)	461 (21 600)	373 (1.25)
18	Acetone	21.0	42.2	369 (28 400)	356 (0.89)	436 (25 000)	372 (1.27)
19	Ethanol	25.3	51.9	374 (32 600)	357 (0.89)	449 (20 000)	371 (1.27)
20	Acetonitrile	36.6	45.6	369 (22 100)	357 (0.89)	435 (23 800)	369 (1.28)
21	DMF	38.3	43.2	373 (29 800)	358 (0.89)	434 (17 400)	367 (1.29)
22	DMSO	47.2	45.1	375 (30 000)	358 (0.89)	433 (21 500)	365 (1.31)

[a] Dielectric constant (ref. 57). [b] Solvent polarity parameter (ref. 5 and 58). [c] No data. [d] **NI2-V** reacts with the solvent to form the pyridinium salts with the ICT-based $\lambda_{max(exp)}^{abs\text{-}solution}$ at 460–480 nm (Fig. S7a, ESI). [e] Poorly soluble. [f] Oscillator strength.

Furthermore, it was found that the $\lambda_{max(exp)}^{abs\text{-}solution}$ of **OD2-V** and **poly(OD2-co-S)** in halopropanes (PrCl, PrBr, and PrI) shows a hypsochromic shift compared to those in halomethanes (CHBr$_3$, CHCl$_3$, CH$_2$I$_2$, CH$_2$Br$_2$, CH$_2$Cl$_2$, and CH$_3$I) and halobenzenes (PhI, PhBr, PhCl, and PhF) although the $\lambda_{max(exp)}^{abs\text{-}solution}$ of **OD2-V** in PrI shows a slight bathochromic shift by 2 nm compared to those in CH$_3$I and PhI (Tables 1 and 2). Meanwhile, the $\lambda_{max(exp)}^{abs\text{-}solution}$ of **OD2-V** and **poly(OD2-co-S)** in pyridine as a protophilic solvent and ethanol as a polar protic solvent appear at a longer wavelength region by *ca.* 30 nm and *ca.* 15 nm, respectively, than those in other non-halogenated solvents. As shown in Fig. 4, the colors of **NI2-V** and **poly(NI2-co-S)** are nearly colorless in all the solvents. Interestingly, the colors of **OD2-V** and **poly(OD2-co-S)** are yellow in non-halogenated solvents but orange in halogenated solvents, especially in CHBr$_3$, CH$_3$I, CH$_2$Br$_2$, and CH$_2$Cl$_2$.

To clarify the influence of solvent polarity on the ICT-based photoabsorption bands of **NI2-V**, **OD2-V**, **poly(NI2-co-S)**, and **poly(OD2-co-S)**, the wavenumbers ($\tilde{\nu}$) of the $\lambda_{max(exp)}^{abs\text{-}solution}$ are plotted against the dielectric constant (ε_r) of the solvent (Fig. 5a, b and 6a, b) or solvent polarity parameter $E_T(30)$ (Fig. 5e, f and 6c, d). The plots for **NI2-V** and **poly(NI2-co-S)** demonstrate that the $\tilde{\nu}$ shows no systematic change and remains on a near plateau in the range of ε_r or $E_T(30)$ value between 1,4-dioxane (no. 1) and DMSO (no. 22) or ethanol (no. 19) (Fig. 5a, e and 6a, c). Thus, the fact indicates that **NI2-V** and **poly(NI2-co-S)** do not possess appreciable solvatochromic properties because for D–π–A type pyridine dyes (**NI2** chromophore), the structural and electronic characteristics of both the ground and Franck–Condon photoexcited states do not differ much with a change in solvent polarity. Meanwhile, the plots

for **OD2-V** and **poly(OD2-co-S)** did not show a systematic change in $\tilde{\nu}$ with increasing $E_T(30)$ or ε_r value and remained on a near plateau between non-halogenated solvents except for pyridine and ethanol, but obviously, the $\tilde{\nu}$ in halogenated solvents are located in the low-wavenumber range compared with those in non-halogenated polar and non-polar solvents (Fig. 5b, f and 6b, d); the ε_r value (7.77) of CH$_2$Br$_2$ is very similar to that (7.52) of THF, and the $\lambda_{max(exp)}^{abs\text{-}solution}$ (473 nm) of **OD2-V** and **poly(OD2-co-S)** in CH$_2$Br$_2$ appears at a longer wavelength region by 39 nm and 28 nm, respectively, than those (434 nm and 445 nm, respectively) in THF. Therefore, the fact evidently indicates that the D–π–A type pyridinium dyes (**OD2** chromophore) possess remarkable organohalogenochromic properties. Moreover, one can see that the $\lambda_{max(exp)}^{abs\text{-}solution}$ of **OD2-V** and **poly(OD2-co-S)** in iodinated solvents, such as PhI, CH$_2$I$_2$, and 1-iodopropane (PrI), occurs at a lower wavenumber range (a longer wavelength region) compared to those in the corresponding chlorinated and brominated solvents. Furthermore, we performed the photoabsorption spectral measurements of **OD2-V** in a mixture of THF as a non-halogenated solvent and CH$_2$Br$_2$ as a halogenated solvent and plotted the $\tilde{\nu}$ of the $\lambda_{max(exp)}^{abs\text{-}solution}$ against the THF/CH$_2$Br$_2$ mixture composition (Fig. S8, ESI†). If the plot shows a curve, the formation of a specific interaction between the dye and the solvent molecules is anticipated.[59,60] However, the plot was almost linear, and thus we could not obtain useful information for intermolecular interactions between the dye and the organohalogen molecules.

Semi-empirical molecular calculations

To reveal the solvatochromism of the D–π–A type pyridine and pyridinium dyes, semi-empirical MO calculations of **NI2-V** and

Table 2 Experimental photophysical data of **poly(NI2-co-S)** and **poly(OD2-co-S)** in various solvents

No.	Solvents	$\varepsilon_r{}^a$	$E_T(30)^b$/kcal mol^{-1}	Poly(NI2-co-S) $\lambda_{max(exp)}^{abs\text{-}solution}$/nm	Poly(OD2-co-S) $\lambda_{max(exp)}^{abs\text{-}solution}$/nm
1	1,4-Dioxane	2.22	36.0	375	443
2	Anisole	4.30	37.1	379	456
3	CHBr$_3$	4.40	37.7	—^{d}	488
4	PhI	4.59	36.2	382	470
5	CHCl$_3$	4.81	39.1	380	479
6	CH$_2$I$_2$	5.32	36.5	—^{d}	—^{e}
7	PhBr	5.45	36.6	379	467
8	PhF	5.47	37.0	377	460
9	PhCl	5.69	36.8	379	464
10	CH$_3$I	6.97	—^{c}	—^{d}	477
11	1-Iodopropane (PrI)	7.07	35.7	380	474
12	THF	7.52	37.4	376	445
13	CH$_2$Br$_2$	7.77	39.4	382	473
14	1-Bromopropane (PrBr)	8.09	36.9	378	456
15	1-Chloropropane (PrCl)	8.59	37.4	376	454
16	CH$_2$Cl$_2$	8.93	40.7	377	475
17	Pyridine	13.3	40.5	378	469
18	Acetone	21.0	42.2	—^{e}	—^{e}
19	Ethanol	25.3	51.9	—^{e}	—^{e}
20	Acetonitrile	36.6	45.6	—^{e}	—^{e}
21	DMF	38.3	43.2	375	444
22	DMSO	47.2	45.1	—^{e}	—^{e}

^{a} Dielectric constant (ref. 57). ^{b} Solvent polarity parameter (ref. 5 and 58). ^{c} No data. ^{d} **Poly(NI2-co-S)** reacts with the solvent to form the pyridinium salts with the ICT-based $\lambda_{max(exp)}^{abs\text{-}solution}$ at 460–480 nm (Fig. S7b, ESI). ^{e} Poorly soluble.
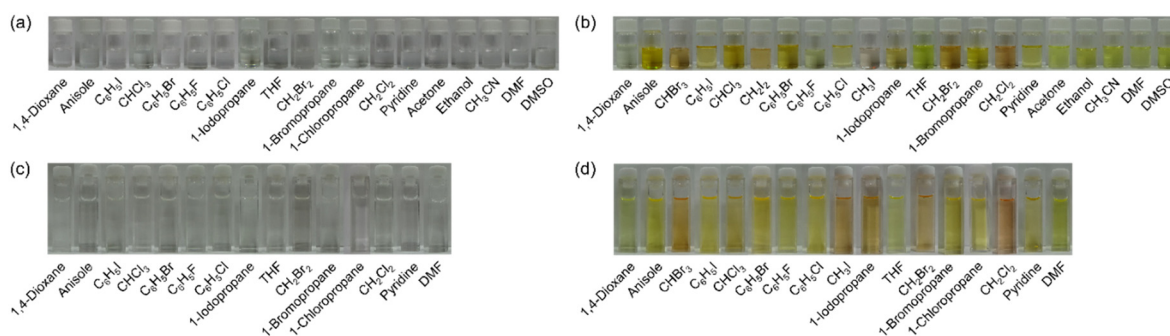

Fig. 4 Photographs of (a) **NI2-V**, (b) **OD2-V**, (c) **poly(NI2-co-S)**, and (d) **poly(OD2-co-S)** in various solvents.

the dye cation for **OD2-V** were performed by applying the INDO/S method, with the SCRF Onsager Model applied after performing geometrical optimizations using the MOPAC/AM1 method. For **NI2-V** and **OD2-V** in all the solvents, the MO calculations show that the first excitation bands are mainly assigned to a transition from the highest occupied molecular orbital (HOMO) to the lowest unoccupied molecular orbital (LUMO) with CI (configuration interaction) component of *ca.* 60% for **NI2-V** and *ca.* 70% for **OD2-V**, where the HOMOs of **NI2-V** and **OD2-V** are mostly localized on the (diphenylamino)carbazole moiety and the LUMOs are mostly localized on the carbazole moiety containing the pyridine ring for **NI2-V** and the pyridinium ring for **OD2-V** (Fig. 7a, b for CH$_2$Cl$_2$, see Fig. S9 and S10 for 1,4-dioxane and DMSO, respectively, ESI†). Thus, the HOMO and LUMO distributions for the molecular structure of **OD2-V** are adequately separated. The changes in the calculated electron density accompanying the first electron excitation demonstrate

that for **OD2-V**, the ICT upon photoexcitation occurs from the (diphenylamino)carbazole unit as a D–π moiety to the pyridinium ring as an A moiety, but for **NI2-V**, the ICT upon photoexcitation occurs from the diphenylamino group as a D moiety to the pyridine ring as an A moiety through the carbazole skeleton as a π-conjugated bridge (Fig. 7c, see Fig. S9 and S10 for 1,4-dioxane and DMSO, respectively, ESI†). The calculated ICT-based photoabsorption maxima ($\lambda_{max(calc)}^{abs\text{-}solution}$ = *ca.* 360 nm) of **NI2-V** appear in a shorter wavelength region compared to those (365–440 nm) of **OD2-V** (Table 1). The corresponding oscillator strength (f) values (*ca.* 1.0–1.3) for **OD2-V** are higher than those (*ca.* 0.9) for **NI2-V**. The plot of the $\lambda_{max(calc)}^{abs\text{-}solution}$ ($\tilde{\nu}$) for NI2-V against the ε_r value of solvent shows that the $\tilde{\nu}$ is constant in the range of ε_r value between 1,4-dioxane (2.22) and DMSO (47.2) (Fig. 5c), indicating that the calculated ICT-based photoabsorption bands of **NI2-V** are independent of solvent polarity. Thus, for **NI2-V**, these calculated results agree with their
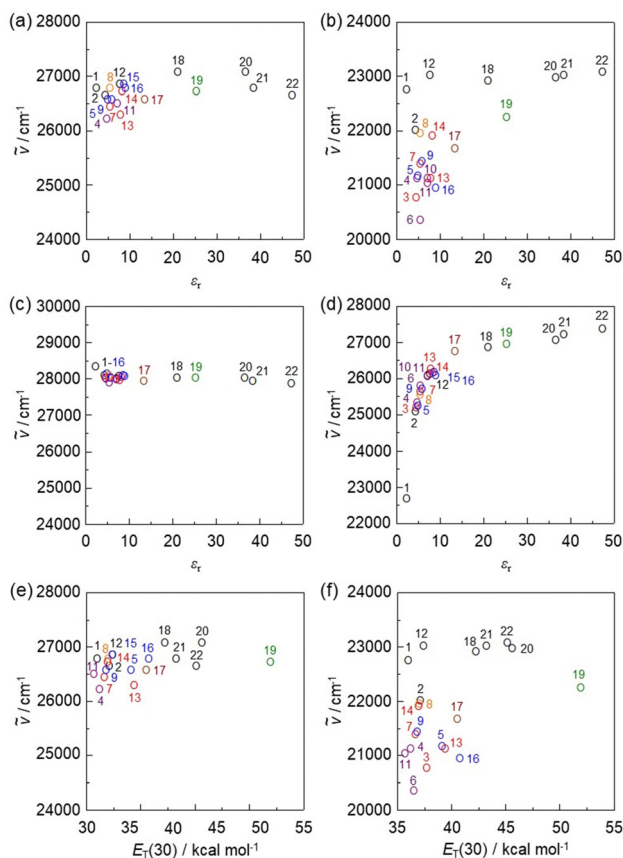
Fig. 5 Plots of the experimental photoabsorption maximum wavenumber ($\tilde{v}$) of (a) **NI2-V** and (b) **OD2-V** against the ε_r value of the solvent. Plots of the calculated $\tilde{v}$ of (c) **NI2-V** and (d) **OD2-V** against the ε_r value of the solvent. Plots of the experimental $\tilde{v}$ of (e) **NI2-V** and (f) **OD2-V** against solvent polarity parameter $E_T(30)$. The numbers correspond to those of Table 1. The circles in black, orange, blue, red, purple, brown, and green show non-halogenated solvents, fluorobenzene, chlorinated solvents, brominated solvents, iodinated solvents, pyridine, and ethanol, respectively.
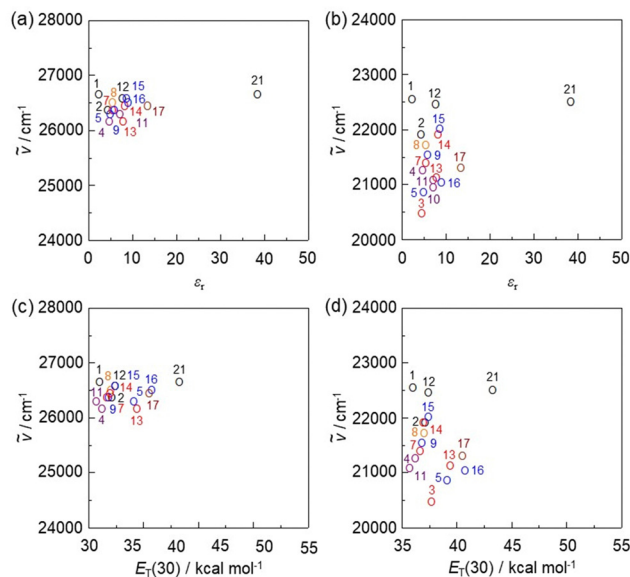

Fig. 6 Plots of the experimental photoabsorption maximum wavenumber ($\tilde{v}$) of (a) **poly(NI2-co-S)** and (b) **poly(OD2-co-S)** against the ε_r value of the solvent. Plots of the experimental $\tilde{v}$ of (c) **poly(NI2-co-S)** and (d) **poly(OD2-co-S)** against solvent polarity parameter $E_T(30)$. The numbers correspond to those in Table 2. The circles in black, orange, blue, red, purple, brown, and green represent non-halogenated solvents, fluorobenzene, chlorinated solvents, brominated solvents, iodinated solvents, pyridine, and ethanol, respectively.
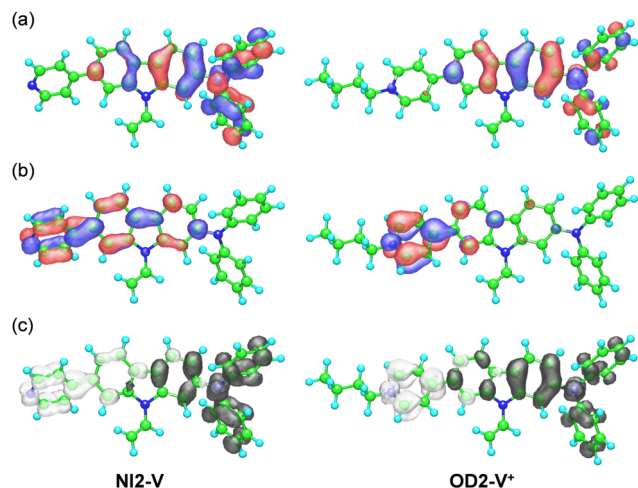

Fig. 7 (a) HOMO and (b) LUMO of **NI2-V** and the dye cation (**OD2-V⁺**) for **OD2-V**. The red and blue lobes denote the positive and negative phases of the coefficients of the molecular orbitals. The size of each lobe is proportional to the MO coefficient. (c) Calculated electron density changes accompanying the first electronic excitation of **NI2-V** and **OD2-V⁺** (by the SCRF Onsager model (solvent = CH$_2$Cl$_2$)). The black and white lobes signify decrease and increase in electron density accompanying the electronic transition, respectively. Their areas indicate the magnitude of the electron density change.

experimental results. However, for **OD2-V**, with increasing solvent polarity from 1,4-dioxane to DMSO, the calculated ICT-based photoabsorption bands show hypsochromic shifts from 440 nm to 365 nm (Table 1). The plot of the $\lambda_{\max(\text{calc})}^{\text{abs-solution}}$ ($\tilde{v}$) for **OD2-V** against the ε_r value demonstrates that the $\tilde{v}$ dramatically increases with the increase in ε_r value from 1,4-dioxane (2.22) to pyridine (13.3), while the $\tilde{v}$ gradually increases with the increase in ε_r value from pyridine to DMSO (47.2) (Fig. 5d). Obviously, for **OD2-V**, the profile of the calculational plot shows a general n-SC, which is significantly different from that of the experimental plot (Fig. 5b).

¹H NMR spectra

To investigate the solvent effect on the electronic structures of **NI2-V** and **OD2-V** in the ground state, we performed ¹H NMR spectral measurements in DMSO-d_6 with a high ε_r value, acetone-d_6 with a moderate ε_r value, and THF-d_8 with a relatively low ε_r value as a non-halogenated solvent, ethanol-d_6 as a polar protic solvent, and pyridine-d_5 as a protophilic solvent,

and in CD$_2$Cl$_2$ and CDCl$_3$ as a halogenated solvent (Fig. 8 and 9). There is a slight difference in the chemical shifts of the aromatic protons for **NI2-V** between the seven solvents, while in pyridine-d_5, the signals for aromatic protons (H$_{a-h}$) of the carbazole skeleton
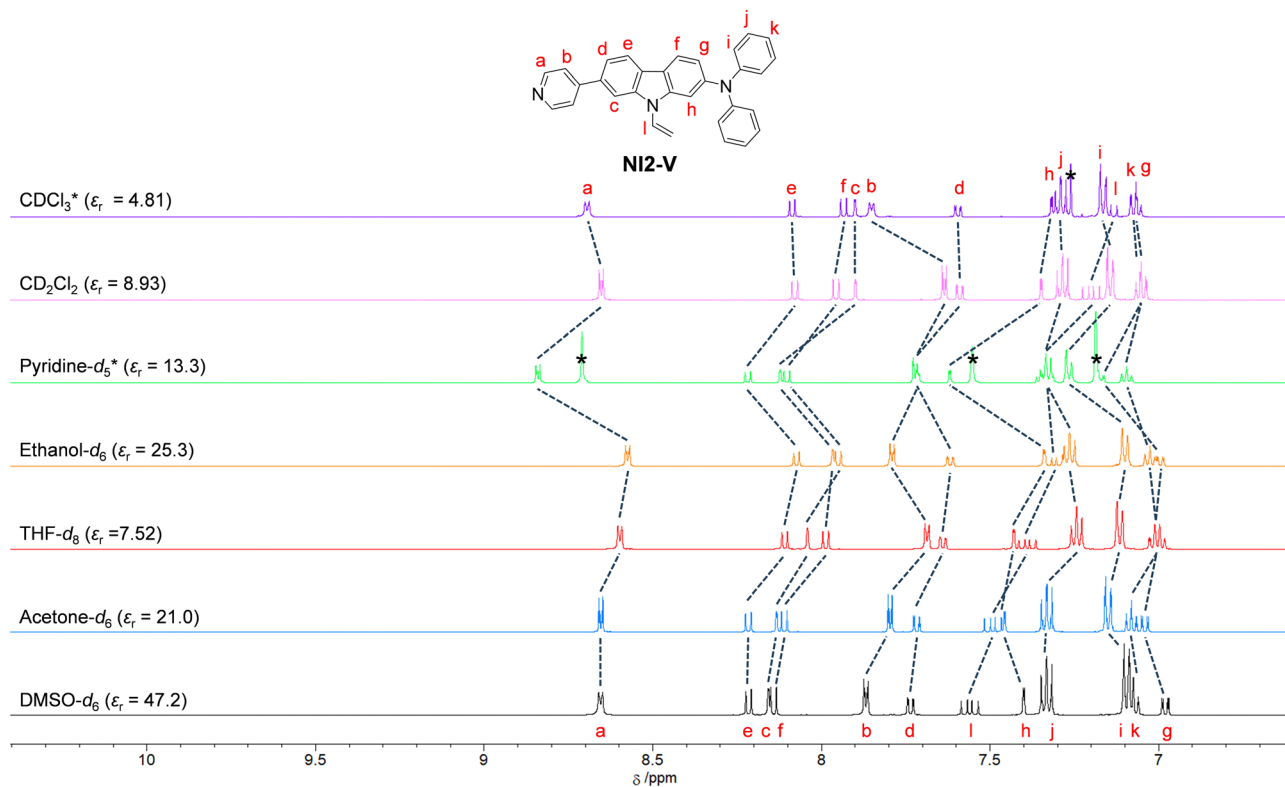
Fig. 8 ^{1}H NMR spectra of **NI2-V** in CDCl$_3$, CD$_2$Cl$_2$, pyridine-d_5, ethanol-d_6, THF-d_8, acetone-d_6, and DMSO-d_6.
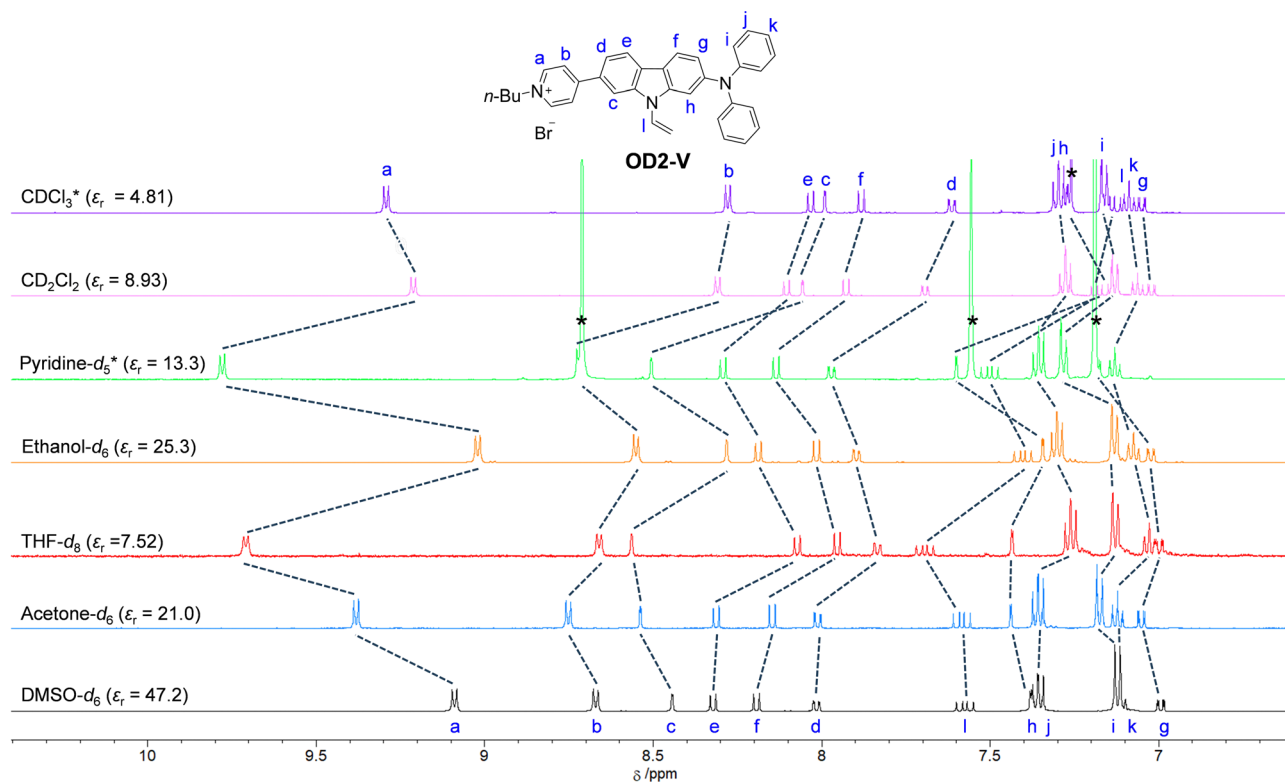
Fig. 9 ^{1}H NMR spectra of **OD2-V** in CDCl$_3$, CD$_2$Cl$_2$, pyridine-d_5, ethanol-d_6, THF-d_8, acetone-d_6, and DMSO-d_6.

and the pyridyl group show downfield shifts compared to those in other solvents. However, for **OD2-V**, considerable differences in the chemical shifts were observed between halogenated and non-halogenated solvents. With decreasing solvent polarity between DMSO-d_6, acetone-d_6, and THF-d_8. The signal for H_a of the pyridinium ring shows downfield shifts, while those for H_c, H_d and H_e of the carbazole skeleton near the pyridinium ring show downfield and upfield shifts. Moreover, the signals for H_a, H_b, and H_c in ethanol-d_6 show upfield shifts, whereas the signal of H_a in pyridine-d_5 shows a downfield shift, compared to those in other non-halogenated solvents. Based on the results of ^{1}H NMR spectral measurements, the bathochromic shifts of the ICT-based photoabsorption band of **OD2-V** in ethanol as a polar protic solvent and pyridine as a protophilic solvent may be due to the enhanced ICT characteristics, which are triggered, respectively, by the formation of hydrogen bonding between the bromide ion of **OD2-V** and the hydroxyl group of ethanol molecules and by the interaction of pyridine molecules with the pyridinium ring of **OD2-V**. It is worth mentioning here that the signals of H_b, H_c, and H_d in CD_2Cl_2 and $CDCl_3$ show considerably upfield shifts compared to those in non-halogenated solvents. Additionally, because the ε_r value of CH_2Cl_2 is similar to that of THF, this result obviously indicates that the chemical shifts for **OD2-V** are not dependent on the solvent polarity but depend on the intermolecular interaction between the D–π–A type pyridinium dyes and the solvent molecules.

Awwadi *et al.* investigated the halogen–halide anion interaction between the halogen atoms of halogenated solvents and the counter halide anion of pyridinium salt based on theoretical and crystallographic studies. They demonstrated that the energy of interaction between the iodine atom of iodinated solvents and halide anion is greater than that of interaction between the chlorine atom in chlorinated solvents or the bromine atom in brominated solvents and the halide anion.[48–50] In fact, the ICT-based photoabsorption bands of **OD2-V** and **poly(OD2-co-S)** in iodinated solvents occur at a lower wavenumber range (a longer wavelength region) compared to those in chlorinated and brominated solvents (Tables 1 and 2), which is accompanied by an increase in the energy of halogen–halide anion interaction. Meanwhile, Matter *et al.* demonstrated the presence of interaction between halogen atoms of the organohalogen compound and aromatic π-systems, that is, halogen–π interaction,[51–55] which plays a crucial role in forming biological, supramolecular, and nanomaterial systems based on biding affinities, X-ray crystal structures, 3D database searches, and *ab initio* calculations.[51] Thus, for **OD2-V**, the large upfield shifts of the signals for protons on the pyridinium and its neighboring aromatic rings from non-halogenated solvent to halogenated solvent are attributable to a change in the electronic structure of **OD2-V** owing to the halogen–halide anion interaction and/or the intermolecular halogen–π interaction between the periphery of the pyridinium moiety of the dyes and the halogen atoms of the organohalogen molecules.

Detection of VOHCs

Next, to evaluate the capability of organohalogenochromic dyes to act in polymer matrices for the visualization and detection

of VOHCs, we prepared drop-casted **poly(OD2-co-S)** films on quartz glass substrates, in which the surfaces were treated with piranha solution and then modified with a hydrophobic monolayer using 1,1,1,3,3,3-hexamethyldisilazane (HMDS) to obtain stable polymer thin films prior to the drop casting, and performed the photoabsorption spectral measurement of the drop-casted **poly(OD2-co-S)** films before and after exposure to non-halogenated and halogenated solvent vapors. In addition, the **poly(NI2-co-S)** films were prepared on the piranha- and HMDS-treated quartz glass substrates using a drop-casting process for comparison with the drop-casted **poly(OD2-co-S)** films. The as-prepared **poly(NI2-co-S)** or **poly(OD2-co-S)** films (in the air) showed an ICT-based photoabsorption band with a $\lambda_{max}^{abs-film}$ of *ca.* 380 nm and *ca.* 450 nm, respectively (Fig. 10), as with the cases of **poly(NI2-co-S)** in non-halogenated and halogenated solvents and **poly(OD2-co-S)** in non-halogenated solvents (Fig. 3). When the **poly(NI2-co-S)** films were exposed to THF, DMF, $CHCl_3$, CH_2Cl_2, or 1-bromopropane (PrBr) vapor (for 2 min in solvent–vapor atmosphere), the ICT-based photoabsorption band did not undergo appreciable changes in the spectral shape and the $\lambda_{max}^{abs-film}$ (Fig. 10a). However, the **poly(OD2-co-S)** films showed a relatively large bathochromic shift of the $\lambda_{max}^{abs-film}$ by *ca.* 10 nm upon exposure to $CHCl_3$ or CH_2Cl_2 vapor (Fig. 10b). When the **poly(OD2-co-S)** films after exposure to the halogenated solvent vapors were placed in the air (on drying), the photoabsorption spectra recovered the original spectral shapes before exposure to the halogenated solvent vapors. Therefore, for **poly(OD2-co-S)** film, the reversibility of the $\lambda_{max}^{abs-film}$ in the $CHCl_3$- and CH_2Cl_2-vapor atmosphere processes was investigated (Fig. 11). It was found that the **poly(OD2-co-S)** films showed good reversible switching of $\lambda_{max}^{abs-film}$ even in the five-time air–vapor cycles, indicating that it is a suitable polymeric functional dye material for the visualization and detection of VOHCs. Actually, one can see that the color of the as-prepared **poly(OD2-co-S)** films is yellow in air or THF-, PrBr- and DMF-vapor atmosphere but is transformed into orange in CH_2Cl_2- and $CHCl_3$-vapor atmosphere (Fig. 12). Moreover, it is worth mentioning here that the **poly(OD2-co-S)** film shows a quick response to VOHCs: the color change in the **poly(OD2-co-S)** film by exposure to CH_2Cl_2- or $CHCl_3$-vapor was completed within 30 s, and then the film recovered the original
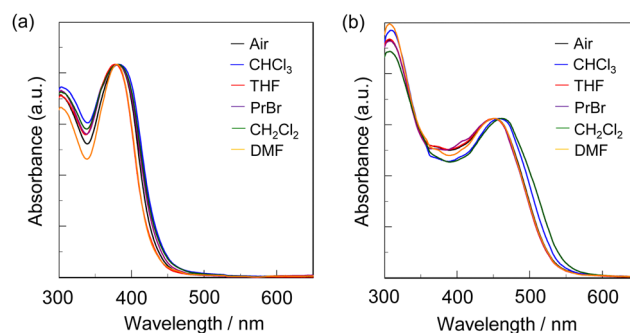

Fig. 10 Photoabsorption spectra of (a) **poly(NI2-co-S)** film and (b) **poly(OD2-co-S)** film in air and solvent–vapor atmosphere.
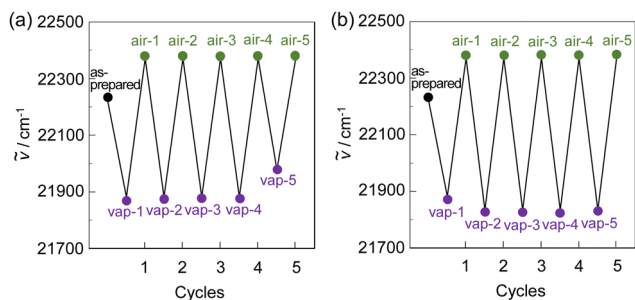
Fig. 11 Reversible switching of photoabsorption maximum wavenumber ($\tilde{v}$) of **poly(OD2-co-S)** film in air and (a) CHCl$_3$- and (b) CH$_2$Cl$_2$-vapor atmosphere processes.
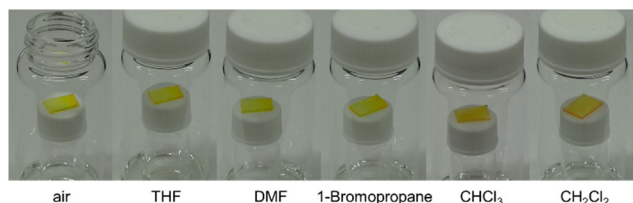

Fig. 12 Photographs of **poly(OD2-co-S)** films in air and solvent–vapor atmosphere.

color within 10 s upon exposure to air at room temperature (see Movie S1 for **poly(OD2-co-S)** film upon exposure to CH$_2$Cl$_2$ vapor, ESI†). Evidently, this result revealed that the D–π–A type pyridinium dyes in polymer matrices can also express b-OHC based on the enhanced ICT characteristics, leading to the destabilization of the HOMO energy level and/or the stabilization of the LUMO energy level, which is induced by the intermolecular interaction between the dye and the organohalogen molecules produced by contact between them. Meanwhile, our previous work demonstrated that **OD3** bearing an iodide ion (I$^-$) as the counter anion shows an obvious b-OHC, compared to **OD1** and **OD2** bearing a chloride anion (Cl$^-$) and a bromide anion (Br$^-$), respectively (Fig. 1a).[2] Thus, to improve the visualization of VOHCs by a huge change in the photoabsorption wavelength in air and the VOHC-vapor atmosphere process, further studies on b-OHC of D–π–A type pyridinium dye polymers bearing various counter anions are required.

Conclusions

We designed and synthesized a D–π–A type pyridinium dye monomer **OD2-V** possessing intramolecular charge transfer (ICT) characteristics and prepared a copolymer **poly(OD2-co-S)** composed of **OD2-V** and styrene to elucidate organohalogenochromism (OHC) and to develop optical polymeric materials for the visualization and detection of volatile organohalogen compounds (VOHCs). It was found that **poly(OD2-co-S)** and **OD2-V** exhibit bathochromic shift-type OHC (b-OHC) in halogenated solvents: **OD2-V** and **poly(OD2-co-S)** show a significant bathochromic shift of ICT-based photoabsorption bands in halogenated solvents, such as dichloromethane (CH$_2$Cl$_2$) and

dibromomethane (CH$_2$Br$_2$), compared with those in non-halogenated solvents. Furthermore, the drop-casted **poly(OD2-co-S)** film shows the bathochromic shift of the ICT-based photoabsorption band in the halogenated solvent–vapor atmosphere, that is, a visual change in color from yellow to orange upon exposure to VOHCs, including chloroform (CHCl$_3$) and CH$_2$Cl$_2$. The **poly(OD2-co-S)** film exhibits good reversible switching of the ICT-based photoabsorption band in the air and VOHC-vapor atmosphere process. The optical sensing properties of **poly(OD2-co-S)** film to VOHCs, and the ^{1}H NMR spectral measurements in non-halogenated and halogenated solvents and semi-empirical molecular calculations for **OD2-V**, revealed that the enhanced ICT characteristics of **OD2** chromophore induced by the intermolecular interaction between the dye and the organohalogen molecules are responsible for the b-OHC of D–π–A type pyridinium dyes. Therefore, this work sufficiently elucidated the b-OHC of D–π–A type pyridinium dyes and demonstrated that polymeric organohalogenochromic dyes are one of the most promising and convenient functional dye materials for colorimetric detection of VOHCs.

Experimental

General

Melting points were measured with an AS ONE ATM-02. IR spectra were recorded using a SHIMADZU IRTracer-100 spectrometer by the ATR method. ^{1}H and ^{13}C NMR spectra were recorded using a Varian-500 FT NMR spectrometer. High-resolution mass spectral data were obtained using APCI and ESI with a Thermo Fisher Scientific LTQ Orbitrap XL. Photoabsorption spectra were observed with a SHIMADZU UV-3600 plus. Polymer number-average molecular weights (M_n) and molecular weight distributions (M_w/M_n) were determined by size exclusion chromatography (SEC) at 40 °C using a SHIMADZU Prominence-i LC-2030 plus with a guard column (LF-G, Shodex), two series-connected columns (LF-804, Shodex), a UV detector, and a differential refractive index detector (RID-20A). THF was used as the eluent, and polystyrene standards were used to calibrate the SEC system.

Synthesis

***N,N*-Diphenyl-7-(pyridin-4-yl)-9-vinyl-9*H*-carbazol-2-amine (NI2-V).** A solution of **NI2** (0.765 g, 1.86 mmol) in dry toluene (30.6 mL) and 1,2-dimethoxyethane (DME) (6.5 mL) under a nitrogen atmosphere was added to a 1.6 M hexane solution of *n*-BuLi (1.74 mL, 2.79 mmol) dropwise and stirred for 30 min at room temperature. Then, bis(dibenzylideneacetone)-palladium(0) (Pd(dba)$_2$) (0.043 g, 0.074 mmol), a 10 wt% hexane solution of tri-*t*-butyl phosphine (0.444 mL, 0.149 mmol), and a 1.0 M ethyl ether solution of vinyl bromide (5.58 mL, 5.58 mmol) were added, and the solution was stirred at 90 °C for 2 h. The resulting mixture was cooled to room temperature, passed through a short column with silica gel (ethyl acetate as eluent) and concentrated. The residue was chromatographed on silica gel (dichloromethane : ethyl acetate = 4 : 1 as eluent) to give **NI2-V**

(0.522 g, yield 64%) as a yellow solid; m.p. 104–106 °C; FT-IR (ATR): $\tilde{v}$ = 3032, 1589, 1487, 1463, 1433, 1273, 1230, 800, 750, 694 cm^{-1}; ^{1}H NMR (500 MHz, acetone-d_6): 5.13 (dd, J = 1.1 and 9.3 Hz, 1H), 5.47 (dd, J = 1.1 and 15 Hz, 1H), 7.04 (dd, J = 1.9 and 8.4 Hz, 1H), 7.06–7.10 (m, 2H), 7.14–7.16 (m, 4H), 7.31–7.35 (m, 4H), 7.46 (d, J = 1.7 Hz, 1H), 7.49 (dd, J = 9.3 and 16 Hz, 1H), 7.72 (dd, J = 1.6 and 8.1 Hz, 1H), 7.80 (dd, J = 1.7 and 4.5 Hz, 2H), 8.11 (d, J = 8.4 Hz, 1H), 8.13 (d, J = 1.0 Hz, 1H), 8.22 (d, J = 8.4 Hz, 1H), 8.65 (dd, J = 1.7 and 4.4 Hz, 2H) ppm; ^{13}C NMR (125 MHz, acetone-d_6): δ = 103.20, 107.05, 109.74, 119.14, 119.83, 120.85, 121.17, 122.20, 122.46, 123.96, 125.15, 125.52, 130.29, 130.51, 136.33, 141.24, 141.97, 148.51, 148.98, 149.16, 151.22 ppm; HRMS (APCI): m/z (%): [M + H]$^+$ calcd for $C_{31}H_{24}N_3$, 438.19647; found 438.19632.

1-Butyl-4-(7-(diphenylamino)-9-vinyl-9H-carbazol-2-yl)pyridinium bromide (OD2-V). A solution of **NI2-V** (0.200 g, 0.457 mmol) and 1-bromobutane (3.95 mL, 36.6 mmol) in dry acetonitrile (50 mL) was stirred for 16 h at 80 °C. After concentrating under reduced pressure, the resulting residue was subjected to reprecipitation from CH_2Cl_2/hexane to give **OD2-V** (0.206 g, yield 78%) as orange solids; m.p. 130–132 °C; FT-IR (ATR): $\tilde{v}$ = 3034, 1616, 1523, 1487, 1465, 1433, 1315, 1263, 802, 752, 694 cm^{-1}; ^{1}H NMR (500 MHz, acetone-d_6): 1.00 (t, J = 7.5 Hz, 3H), 1.46–1.54 (m, 2H), 2.10–2.17 (m, 2H), 4.92 (t, J = 7.5 Hz, 2H), 5.16 (dd, J = 1.1 and 9.2 Hz, 1H), 5.49 (dd, J = 1.2 and 16 Hz, 1H), 7.05 (dd, J = 1.9 and 8.5 Hz, 1H), 7.10–7.14 (m, 2H), 7.17–7.19 (m, 4H), 7.34–7.37 (m, 4H), 7.44 (d, J = 1.8 Hz, 1H), 7.58 (dd, J = 9.2 and 15.9 Hz, 1H), 8.01 (dd, J = 1.7 and 8.3 Hz, 1H), 8.15 (d, J = 8.5 Hz, 1H), 8.31 (d, J = 8.2 Hz, 1H), 8.54 (d, J = 0.1 Hz, 1H), 8.75 (d, J = 7 Hz, 2H), 9.38 (d, J = 7.1 Hz, 2H) ppm; ^{13}C NMR (125 MHz, CDCl$_3$): δ = 13.68, 19.54, 33.57, 60.80, 104.89, 105.33, 109.76, 117.58, 118.23, 120.36, 120.76, 121.81, 123.70, 124.61, 124.99, 127.85, 129.07, 129.55, 129.58, 140.25, 142.24, 144.59, 147.74, 149.00, 156.78 ppm; HRMS (ESI†): m/z (%): [M–Br]$^+$ calcd for $C_{35}H_{32}N_3$, 494.25907; found 494.25894.

Preparation of poly(NI2-co-S)

NI2-V (0.378 g, 0.864 mmol), styrene (9.40 mL, 99.6 mmol), and azobis(isobutyronitrile) (0.071 mg, 0.43 mmol) were degassed with nitrogen bubbling, and then the solution was stirred for 5 h at 60 °C under nitrogen atmosphere. The reaction mixture was dissolved in dichloromethane. The dichloromethane solution was poured into n-hexane, and the resulting precipitate was collected to give **poly(NI2-co-S)** (0.902 g, yield 8%) as a white solid; m.p. 131–150 °C; FT-IR (ATR): $\tilde{v}$ = 3024, 1600, 1492, 1452, 1028, 906, 754, 696 cm^{-1}; ^{1}H NMR (500 MHz, THF-d_8): 1.49 (br, CH$_2$-C$\underline{H}$ for styrene and **NI2-V** unit), 1.89 (br, CH-C$\underline{H}_2$ for styrene and **NI2-V** unit), 6.61 (br, C$\underline{H}$ on Ph for styrene), 7.07 (br, C$\underline{H}$ on Ph for styrene), 7.89 (br, aromatic protons for **NI2-V** unit), and 8.57 (br, C$\underline{H}$ on pyridine ring for **NI2-V** unit) ppm. The molar ratio (x/y) of styrene unit (x) and **NI2-V** unit (y) and the weight percentage (wt%) of **NI2-V** unit were determined to be $ca.$ 667 and $ca.$ 0.62 wt%, respectively, from the ^{1}H NMR spectrum; SEC M_n = 59 200, M_w/M_n = 1.55.

Preparation of poly(OD2-co-S)

Poly(NI2-co-S) (0.500 g, 8.5 × 10^{-3} mmol) and 1-bromobutane (5.0 mL, 47 mmol) were stirred for 1 day at 100 °C. The reaction

mixture was concentrated, and the resulting residue was dissolved in dichloromethane. The dichloromethane solution was poured into n-hexane, and the resulting precipitate was collected to give **poly(OD2-co-S)** (0.423 g, yield 84%) as a yellow solid; m.p. 140–174 °C; FT-IR (ATR): $\tilde{v}$ = 3024, 1600, 1492, 1452, 1028, 906, 754, 694 cm^{-1}; ^{1}H NMR (500 MHz, THF-d_8): 1.49 (br, CH$_2$-C$\underline{H}$ for styrene and **OD2-V** unit), 1.90 (br, CH-C$\underline{H}_2$ for styrene and **OD2-V** unit), 5.01 (br, N-C$\underline{H}_2$-CH$_2$ of butyl group for **OD2-V** unit), 6.61 (br, C$\underline{H}$ on Ph for styrene), 7.07 (br, C$\underline{H}$ on Ph for styrene), 7.78 (br, aromatic protons for **OD2-V** unit), and 9.56 (br, C$\underline{H}$ on pyridinium ring for **OD2-V** unit) ppm.

Preparation of poly(NI2-co-MMA) and poly(OD2-co-S) films

A solution of **poly(NI2-co-S)** (0.100 g) in THF (2.0 mL) or **poly(OD2-co-S)** (0.075 g) in THF (1.5 mL) was stirred for 15 h at room temperature. To prepare a polymer film, 250 µL of the polymer solution was drop-casted on a treated quartz glass substrate, where the surfaces of the quartz glass substrate were treated with piranha solution and then modified with a hydrophobic monolayer using 1,1,1,3,3,3-hexamethyldisilazane (HMDS) to obtain stable polymer thin films prior to drop casting. The drop-casted films were dried under a nitrogen atmosphere for 30 min. The resulting **poly(NI2-co-S)** or **poly(OD2-co-S)** films were exposed to solvent vapor for 2 min (in the solvent–vapor atmosphere) to perform the photoabsorption spectral measurements with a calibrated integrating sphere system.

Computational methods

The semi-empirical calculations were carried out with the WinMOPAC Ver. 3.9 package (Fujitsu, Chiba, Japan). The geometry calculation of compounds in the ground state was performed using the AM1 method. The geometry was completely optimized (keyword PRECISE) by the eigenvector following routine (keyword EF). The experimental absorption spectra of the compound were compared with their absorption data using the semi-empirical method INDO/S (intermediate neglect of differential overlap/spectroscopic) and the SCRF Onsager Model. All INDO/S calculations were performed using single excitation full SCF/CI (self-consistent field/configuration interaction), which includes the configuration with one electron excited from any occupied orbital to any unoccupied orbital, where 225 configurations were considered [keyword CI (15 15)].

Author contributions

Y. O. conceived the project and directed the experimental studies. K. I. conducted the preparation and analysis of polymer. K. K. performed almost all the experiments and carried out MO calculations. The manuscript was written through contributions of all authors.

Conflicts of interest

There are no conflicts to declare.

Acknowledgements

References

1 T. Higashino and Y. Ooyama, *Chem. Lett.*, 2021, **50**, 1530–1533.

2 Y. Ooyama, Y. Oda, T. Mizumo and J. Ohshita, *Tetrahedron*, 2013, **69**, 1755–1760.

3 Y. Ooyama, K. Kushimoto, Y. Oda, D. Tokita, N. Yamaguchi, S. Inoue, T. Nagano, Y. Harima and J. Ohshita, *Tetrahedron*, 2012, **68**, 8577–8580.

4 Y. Ooyama, R. Asada, S. Inoue, K. Komaguchi, I. Imae and Y. Harima, *New J. Chem.*, 2009, **33**, 2311–2316.

5 C. Reichardt, *Solvents and Solvent Effects in Organic Chemistry*, Wiley-VCH, Weinheim, 2003.

6 I. Bolz, D. Schaarschmidt, T. Rüffer, H. Lang and S. Spange, *Angew. Chem., Int. Ed.*, 2009, **48**, 7440–7443.

7 L. Giordano, V. V. Shvadchak, J. A. Fauerbach, E. A. Jares-Erijman and T. M. Jovin, *J. Phys. Chem. Lett.*, 2012, **3**, 1011–1016.

8 M. Vidal, C. Pastenes, M. Caroli Rezende, C. Aliaga and M. Domínguez, *Org. Chem. Front.*, 2019, **6**, 3896–3901.

9 J. A. Balam-Villarreal, B. J. López-Mayorga, D. Gallardo-Rosas, R. A. Toscano, M. P. Carreón-Castro, V. A. Basiuk, F. Cortés-Guzmán, J. G. López-Cortés and M. C. Ortega-Alfaro, *Org. Biomol. Chem.*, 2020, **18**, 1657–1670.

10 V. Castro-Castillo, J. Gajardo, C. Sandoval-Altamirano, E. Gratton, S. Sanchez, L. Malacrida and G. Gunther, *J. Mater. Chem. B*, 2020, **8**, 88–99.

11 T. Mukherjee, R. J. Martinez-Sanchez, K. T. Fam, S. Bou, L. Richert, D. Garnier, Y. Mély, S. Kanvah, A. S. Klymchenko and M. Collot, *Mater. Chem. Front.*, 2021, **5**, 2459–2469.

12 M. Piejko, B. Patrahau, K. Joseph, C. Muller, E. Devaux, T. W. Ebbesen and J. Moran, *J. Am. Chem. Soc.*, 2023, **145**, 13215–13222.

13 T. Katoh, Y. Inagaki and R. Okazaki, *J. Am. Chem. Soc.*, 1998, **120**, 3623–3628.

14 T. Katoh, K. Ogawa, Y. Inagaki and R. Okazaki, *Bull. Chem. Soc. Jpn.*, 1997, **70**, 1109–1114.

15 B. J. Coe, J. A. Harris, J. J. Hall, B. S. Brunschwig, S.-T. Hung, W. Libaers, K. Clay, S. J. Coles, P. N. Horton, M. E. Light, M. B. Hursthouse, J. Garín and J. Orduna, *Chem. Mater.*, 2006, **18**, 5907–5918.

16 F. Dumur, C. R. Mayer, E. Dumas, F. Miomandre, M. Frigoil and F. Sécheresse, *Org. Lett.*, 2008, **10**, 321–324.

17 T. Kolev, T. Tsanev, S. Kotov, H. Mayer-Figge, M. Spiteller, W. S. Sheldrick and B. Koleva, *Dyes Pigm.*, 2009, **82**, 95–101.

18 T. Dentani, Y. Kubota, K. Funabiki, J. Jin, T. Yoshida, H. Minoura and M. Matsui, *New J. Chem.*, 2009, **33**, 93–101.

19 A. Baheti, P. Singh and K. R. J. Thomas, *Dyes Pigm.*, 2011, **88**, 195–203.

20 M.-A. Tehfe, F. Dumur, B. Graff, F. Morlet-Savary, D. Gigmes, J.-P. Fouassier and J. Lalevée, *Polym. Chem.*, 2013, **4**, 3866–3875.

21 M. Hagimori, N. Mizunuma, K. Yokota, Y. Nishimura, M. Suzuta, C.-K. Tai, B.-C. Wang, S.-L. Wang, T.-L. Shih, H.-H. Wu, K. Kawashima, S. Kawashima and Y. Tominaga, *Dyes Pigm.*, 2012, **92**, 1069–1074.

22 M. Fakis, P. Hrobárik, E. Stathatos, V. Giannetas and P. Persephonis, *Dyes Pigm.*, 2013, **96**, 304–312.

23 A. Gandioso, M. Palau, R. Bresolí-Obach, A. Galindo, A. Rovira, M. Bosch, S. Nonell and V. Marchán, *J. Org. Chem.*, 2018, **83**, 11519–11531.

24 M. Vidal, M. C. Rezende, C. Pastene, C. Aliaga and M. Domínguez, *New J. Chem.*, 2018, **42**, 4223–4231.

25 A. Cesaretti, P. Foggi, C. G. Fortuna, F. Elisei, A. Spalletti and B. Carlotti, *J. Phys. Chem. C*, 2020, **124**, 15739–15748.

26 S. Karmakar, A. Ambastha, A. Jha, A. Dharmadhikari, J. Dharmadhikari, R. Venkatramani and J. Dasgupta, *J. Phys. Chem. Lett.*, 2020, **11**, 4842–4848.

27 G. Prévot, T. Bsaibess, J. Daniel, C. Genevois, G. Clermont, I. Sasaki, S. Marais, F. Couillaud, S. Crauste-Manciet and M. Blanchard-Desce, *Nanoscale Adv.*, 2020, **2**, 1590–1602.

28 A. Kayama, A. Shimizu and R. Shintani, *Synthesis*, 2021, 4042–4047.

29 W. Zeng and J. Wu, *Mater. Chem. Front.*, 2019, **3**, 2668–2672.

30 T.-C. Lin, Z.-Y. Liu, S.-H. Liu, I. O. Koshevoy and P.-T. Chou, *JACS Au*, 2021, **1**, 282–293.

31 R. W. C. Li, L. Ventura, J. Gruber, Y. Kawano and L. R. F. Carvalho, *Sens. Actuators B*, 2008, **131**, 646–651.

32 T. Kakuta, R. Nakanishi, T. Ogoshi and T. Yamagishi, *RSC Adv.*, 2020, **10**, 12695–12698.

33 R. M. El-Shishtawy, F. A. M. Al-Zahrani, S. M. Afzal, M. A. N. Razvi, Z. M. Al-amshany, A. H. Bakry and A. M. Asiri, *RSC Adv.*, 2016, **6**, 91546–91556.

34 K. Ponnusamy, S. Chellappan, C. M. Singaravelu and J. Kandasamy, *J. Lumin.*, 2018, **202**, 253–262.

35 M. Shibayama, Y. Uehashi, S. Ajioka, Y. Kubota, T. Inuzuka and K. Funabiki, *New J. Chem.*, 2023, **47**, 5262–5269.

36 W. Yin, H. Li, A. S. R. Chesman, B. Tadgell, A. D. Scully, M. Wang, W. Huang, C. R. McNeill, W. W. H. Wong, N. V. Medhekar, P. Mulvaney and J. J. Jasieniak, *ACS Nano*, 2021, **15**, 1454–1464.

37 I. Lee, J. E. Kwon, Y. Kang, K. C. Kim and B.-G. Kim, *ACS Sens.*, 2018, **3**, 1831–1837.

38 M. M. Bordbar, J. Tashkhourian and B. Hemmateenejad, *ACS Sens.*, 2019, **4**, 1442–1451.

39 N. Meher, D. Barman, R. Parui and P. K. Iyer, *J. Mater. Chem. C*, 2022, **10**, 10224–10254.

40 A. D. Tjandra, A.-H. Pham and R. Chandrawati, *Chem. Mater.*, 2022, **34**, 2853–2876.

41 T. Eaidkong, R. Mungkarndee, C. Phollookin, G. Tumcharern, M. Sukwattanasinitt and S. Wacharasindhu, *J. Mater. Chem.*, 2012, **22**, 5970–5977.

42 S. Dolai, S. K. Bhunia, S. S. Beglaryan, S. Kolusheva, L. Zeiri and R. Jelinek, *ACS Appl. Mater. Interfaces*, 2017, **9**, 2891–2898.

43 H. Lin, M. Jang and K. S. Suslick, *J. Am. Chem. Soc.*, 2011, **133**, 16786–16789.

44 C. Lu, S. Liu, J. Xu, Y. Ding and G. Ouyang, *Anal. Chim. Acta*, 2016, **902**, 205–211.

45 P. Chen, Y. Tseng, Y. Chuang and J. Chen, *J. Chromatogr. A*, 2015, **1395**, 41–47.

46 S. Das, P. Sharma, P. M. Badani and R. K. Vatsa, *RSC Adv.*, 2015, **5**, 8887–8894.

47 S. Ampuero and J. O. Bosset, *Sens. Actuators B*, 2003, **94**, 1–12.

48 F. F. Awwadi, R. D. Willett, K. A. Peterson and B. Twamley, *Chem. – Eur. J.*, 2006, **12**, 8952–8960.

49 F. F. Awwadi, R. D. Willet, K. A. Peterson and B. Twamley, *J. Phys. Chem. A*, 2007, **111**, 2319–2328.

50 R. D. Willett, F. F. Awwadi and R. Butcher, *Cryst. Growth Des.*, 2003, **3**, 301–311.

51 H. Matter, M. Nazaré, S. Güssregen, D. W. Will, H. Schreuder, A. Bauer, M. Urmann, K. Ritter, M. Wagner and V. Wehner, *Angew. Chem., Int. Ed.*, 2009, **48**, 2911–2916.

52 H. G. Wallnoefer, T. Fox, K. R. Liedl and C. S. Tautermann, *Phys. Chem. Chem. Phys.*, 2010, **12**, 14941–14959.

53 A. Forni, S. Pieraccini, S. Rendine, F. Gabas and M. Sironi, *ChemPhysChem*, 2012, **13**, 4224–4234.

54 A. Forni, S. Pieraccini, S. Rendine and M. Sironi, *J. Comput. Chem.*, 2014, **35**, 386–394.

55 I. S. Youn, D. Y. Kim, W. J. Cho, J. M. L. Madridejos, H. M. Lee, M. Kolaski, J. Lee, C. Baig, S. K. Shin, M. Filatov and K. S. Kim, *J. Phys. Chem. A*, 2016, **120**, 9305–9314.

56 Y. Ooyama, S. Inoue, T. Nagano, K. Kushimoto, J. Ohshita, I. Imae, K. Komaguchi and Y. Harima, *Angew. Chem., Int. Ed.*, 2011, **50**, 7429–7433.

57 *CRC Handbook of Chemistry and Physics*, ed. J. R. Rumble, CRC Press, Boca Raton, 103rd edn, 2022.

58 J. P. Cerón-Carrasco, D. Jacquemina, C. Laurence, A. Planchat, C. Reichardt and K. Sraïdi, *J. Phys. Org. Chem.*, 2014, **27**, 512–518.

59 J. O. Morley, R. M. Morley, R. Docherty and M. H. Charlton, *J. Am. Chem. Soc.*, 1997, **119**, 10192–10202.

60 P. Jacques, *J. Phys. Chem.*, 1986, **90**, 5535–5539.